CHAPTER VI
SYNTHESIS OF MESOPOROUS Si-MCM-41 AND Si-MCM-48 AT ROOM TEMPERATURE AND THEIR CATALYTIC ACTIVITY IN WASTE TIRE PYROLYSIS: EFFECT OF PORE STRUCTURE

6.1 Abstract

Due to a high concentration of large-size molecules, especially aromatic compounds in tire-derived oil, mesoporous catalysts were thus applied in catalytic pyrolysis of waste tire. The objective was to study the effect of pore structure of mesoporous materials on heavy compound removal. The synthesis methods of mesoporous Si-MCM-41 (hexagonal structure) and Si-MCM-48 (cubic structure) at room temperature were adopted in this work. The mesoporous catalysts were synthesized in ethanol and ammonia solutions using tetraethylorthosilicate as a silica source and cetyltrimethylammonium bromide as a template. The solutions were subsequently stirred for 3 hr for Si-MCM-41 and 4 hr for Si-MCM-48. Small-angled X-ray scattering, scanning electron microscopy, and Brunualer-Emmett-Teller instruments were performed to characterize the synthetic materials. Then, the two catalysts were tested in the catalytic pyrolysis of waste tire, operated in a batch reactor. GC×GC-TOF/MS and SIMDIST-GC instruments were used to analyze the liquid products for their chemical compositions and petroleum fraction, respectively. The results showed that the crystallinity of the catalysts was well uniformed. Both catalysts can highly decrease gas oil and vacuum gas oil fractions, leading to an extreme enhancement of gasoline and kerosene. This is due to the large pore sizes of the materials, providing a high diffusion of large-size molecules into a pore. The catalytic cracking reactions were thus greatly occurred. However, the cubic structure gave greater removal of heavy compounds because its three-dimensional interconnected cubic pore structure performed cracking with a higher retention time inside its pore. In addition, the reduction of multi-ring aromatics resulted in the enhancement of mono-aromatic formation. In-depth analysis of mono-aromatic formation was done and discussed in this work as well. Furthermore, these two materials can also extremely reduce sulfur contents in oil.

6.2 Introduction

Advances in oil industry can raise the price of a newly-developed oil that can greatly perform in an engine. Therefore, the improvement of new unconventional sources of fuels has become highly competitive. Tire-derived oil (TDO) is one type of the attractive fuels since it can be obtained from waste tire pyrolysis that can also facilitate usages of waste tire until its end of life. The components in tire-derived oil can be used as chemical feedstock due to a high concentration of mono-aromatics (Yuwapornpanit and Jitkarnka, 2015). However, tire-derived oil cannot be directly used in a vehicle engine because of its off-spec aromatic concentration (Dũng *et al.*, 2009a). The chemical components in maltene of tire-derived oil, analyzed using a two dimensional gas chromatograph with time of-flight mass spectrometry (GCxGC/TOF-MS), were classified into 8 groups based on their structures; that are, saturated hydrocarbon (SATs), olefins (OLEs), naphthenes (NAPs), terpenes (TERs), mono-aromatics (MAHs), poly-aromatics (PAHs) and polar-aromatics (PPAHs) (Pithakratanayothin and Jitkarnka, 2014). It was found that tire-derived oil from thermal pyrolysis contained 60-65 % heavy fractions (gas oil and LVGO, and HVGO) and specifically 20-25 % aromatics (DAHs, PAHs, and PPAHs) (Yuwa-pornpanit and Jitkarnka, 2015). Additionally, approximately 63.1 % of large-size hydrocarbons (> 8 Å), including 45.6 % aromatics (MAHs, DAHs, PPAHs, and PPAHs), 12.5 % aliphatics (SATs and OLEs), and 5.0 % alicyclics (NAPs and TERs), are mostly distributed in gas oil, LVGO, and HVGO fractions (Seng-eiad and Jitkarnka, 2015). Furthermore, their average maximum diameters ($Ø_{m,avg}$) were mostly in the range of 8-16 Å. Thus, catalysts with pore size in the range of 20-30 nm were suggested for reducing these bulky aromatic compounds.

The synthesis of new mesoporous family (M41S), including MCM-41 and MCM-48, was designated in 1992 by Mobil Oil Corporation. These materials are mainly composed of silica wall with uniform structure, high surface area, high pore volume, and constant pore diameters ranging from 2 to 10 nm. MCM-41 has been reported as a well-ordered hexagonal mesoporous silica whereas MCM-48 has a cubic structure. Hydrothermal synthesis via co-condensation is normally adopted to synthesize these materials, which however possess less ordered mesoporous

structure, long-time aging, and high cost of energy usage. Thus, a novel synthesis method at room temperature, which was recently discovered, is more attractive due to short-time aging, low energy usage, high thermal stability, and high uniform structure (Meléndez-Ortiz *et al.*, 2014; Kibombo *et al.*, 2014). The materials were prepared in a base condition at room temperature by adding aqueous NH_4OH and ethanol. Jin *et al.* (2012) stated that the synthetic MCM-41 can be used to crack polystyrene, resulting in a high catalytic activity and a good selectivity to styrene monomer. The co-products were ethylbenzene, isopropylbenzene, isopropenylbenzene and secondary cross-linked compounds. Furthermore, when doped into MCM-41, Ru metal resulted in a enhancement of naphtha and kerosene fractions. This is due to a high conversion of poly- and polar-aromatics into mono-aromatics. Witpathomwong *et al.* (2011) found that Ru/MCM-48 can be used to improve light olefin and light oil productions in tire-derived oil. Furthermore, Ru/MCM-48 insignificantly reduced the amount of sulfur in oil, indicating that it can break bond of C-S. To our knowledge, the effects of pore structure of mesoporous materials on removal of large-size poly- and polar-aromatics and formations of highly-valuable mono-aromatics in TDO from waste tire pyrolysis have not been studied. In this work, the effect of pore structure on the products of tire-derived oil was thus investigated using Si-MCM-41 (hexagonal structure) and Si-MCM-48 (cubic stricture) molecular sieve as catalysts. Firstly, the synthesis of mesoporous Si-MCM-41 and Si-MCM-48 and their properties were studied. Then, the synthetic materials were used in catalytic pyrolysis of waste tire. Furthermore, the formation of valuable petrochemicals and their productivity were focused and discussed in-depth. Lastly, the hetero-atom removal was also observed in this work.

6.3 Experimental

6.3.1 Synthesis of Si-MCM-41 and Si-MCM-48

Tetraethylorthosilicate (TEOS, 99 %, Merck), cetyltrimethylammonium bromide (CTAB, 99 +%, Aldrich), ethanol (EtOH, AR grade, RCI Labscan), aqueous ammonia solution (NH_4OH, 30 %, Merck), and deionized water were used to prepare Si-MCM-41 and Si-MCM-48. A synthetic method at room temperature

was firstly applied to synthesize Si-MCM-41 and Si-MCM-48 in this research work. Si-MCM-41 material was synthesized using the procedure of Meléndez-Ortiz *et al.* (2014). In the synthesis, 0.5 g of CTAB was added to 96 mL of deionized H_2O with the stirring rate of 300 rpm. After the solution become clear (~ 10 min), 34 mL of EtOH and 10 mL of aq. NH_4OH were added to the solution under 5 min stirring. After that, 2 mL of TEOS was poured into the mixture with subsequent stirring for 3 h at room temperature. Si-MCM-48 was prepared using the procedure of Kibombo *et al.* (2014), which is similar to the synthetic method of Si-MCM-41. Briefly, 50 mL of deiorized H_2O, 1.2 g of CTAB, 25 mL of ethanol, 18 mL of aq. NH_4OH, and 1.8 mL of TEOS were mixed under the stirring rate of 300 rpm for 4 h. Then, Si-MCM-41 and Si-MCM-48 were washed until pH 7, and subsequently dried at 105 ^oC overnight. The surfactant template was removed from the solid products by calcinations at 550 ^oC with the heating rate of 2 ^oC/min for 6 h. The obtained Si-MCM-41 and Si-MCM-48 were pelletized, and then sieved to obtain a particle size in the range of 40-60 mesh prior to use.

6.3.2 Catalyst Characterization

The x-ray diffraction (XRD) patterns at low angles were acquired to confirm the structures of Si-MCM-41 and Si-MCM-48. The diffractograms were recorded on a Riguku D/Max2200H apparatus with 50 kW, 300 mA Cu anode in a long fine focus ceramic X-ray tube for generating a CuKα radiation (1.5405 Å) with the scanning speed of 2 ^{o}/min and 2θ from 1^o to 7^o. Field Emission-Scanning Electron Microscope (FE-SEM), Hitachi Model S4800, was utilized to identify the morphology of mesoporous materials. Temperature-programmed desorption (TPD) using NH_3 was carried out in a TPD/TPR Micromeritics 2900 machine to characterize total acidity. The nitrogen adsorption–desorption analysis using ThermoFinnigan/Sorptomatic1990 instrument was performed to determine specific surface area, pore volume and average pore size of the mesoporous materials. The specific surface area was determined using BET method. The average pore size and the pore size distribution were calculated through the BJH method. Before the analysis, approximately 0.1 g of sample was degassed at 250 ^oC for 12 h. In addition, Thermogravimetric/Differential Thermal Analysis (TG/DTA) was used to determine

the degradation of fresh catalyst, and the deposition of coke on spent catalysts. The temperature was ramped from 30 °C to 900 °C with the heating rate of 10 °C/min under 20 mL of oxygen.

6.3.3 Pyrolysis of Waste Tire

The pyrolysis reactor was divided into 2 zones as the same process in Yuwapornpanit and Jitkarnka (2015). The upper zone was catalytic zone (350 °C) and the lower zone was the pyrolytic zone (500 °C). Waste automobile tire (Bridgestone TURANZA GR-80) was first scraped, and then sieved to obtain the small particle size in the range of 20-40 mesh. Firstly, 30 g of the waste tire sample was loaded into the lower zone, and 7.5 g of pellet catalyst was loaded into the catalytic zone. Then, tire sample was heated with the heating rate of 10 °C/min from the room temperature to 500 °C under 30 ml/min nitrogen pressure, and subsequently held for 120 min at final temperature. The gas products were carried out to two condensers for condensing the liquid product, and the other incondensable gas was collected in the sampling gas bag.

6.3.4 Products Analysis

The contents of carbon and hydrogen in liquid products were acquired from using LECO®Elemetal Analyzer (TruSpec®S). The gas compositions were detected using a Gas Chromatography (GC-FID), Agilent Technologies 6890 Network GC system (HP-PLOT Q column: 20 μm film thickness and 30 m × 0.32 mm ID). The liquid product was firstly dissolved in *n*-pentane in the oil/*n*-pentane mass ratio of 40:1 for precipitating asphaltene. After that, the asphaltene was filtered using polyamide membrane (pore size: 0.45μm). The obtained liquid is called maltene. The 30 μL maltene was diluted in the 2 mL carbon disulfide (CS_2) prior to analysis using GC instruments. The true boiling point curves were determined using a Varian GC-3800 simulated distillation gas chromatograph (SIMDIST-GC) conformed to the ASTM-D2887 method. The instrument was equipped with FID and WCOT fused silica capillary column (15 m × 0.25 mm ID × 0.25 μm film thichness). The true boiling point curves were cut into petroleum fractions according to their boiling points; gasoline (< 149 °C), kerosene (149-232 °C), gas oil (232-343 °C),

light vacuum gas oil (343-371 °C) and heavy vacuum gas oil (> 371 °C). Finally, the chemical composition of maltene solution was indentified using a comprehensive two-dimensional Gas Chromatography with Time of Flight Mass Spectrometer (GC×GC/TOF-MS). GC×GC-TOF/MS apparatus equipped an Agilent gas chromatograph 7890 (Agilent Technologies, Palo Alto, CA, USA), a Pegasus® 4D TOF/MS (LECO, St. Joseph, MI, USA) and a thermal modulator was used to analyzed oil compositions. The instrument was operated by the cooperation of two GC columns. The 1st GC column was a non-polar Rtx®-5Sil MS and the 2nd GC column was a polar Rxi®-17 MS. Total Ion Chromatograms (TICs) of maltenes obtained from GCxGC/TOF-MS were plotted in forms of 2D (Contour Plots) and 3D (Surface Plots) in order to observe the distribution of hydrocarbon groups in the chromatograms. The external standard (PIANO, Spectrum Quality Standards, Ltd.) containing benzene (2.425 wt%), toluene (2.576 wt%), ethylbenzene (2.504 wt%), p-xylene (3.374 wt%), and cumene (1.864 wt%) was used for calibrating the peaks of petrochemical products (BTEXC). The PIANO standard was firstly diluted in CS_2 in the PIANO standard/CS_2 volume ratio of 1:10 and then the 30 μL diluted standard was further diluted in 2 mL CS_2 prior to analysis with GCxGC/TOF-MS instruments.

6.3.5 Determination of Sampling Size

According to Israel (2013), the sampling size (n) of hydrocarbon in each molecular group was determined using Yamane method as seen in Eq. (6.1), where N is the population of hydrocarbons in each group, and a ninety percent confidence level was assumed for this equation (e = 0.1). Then, the representative species were estimated the molecular compositions in each petroleum cuts using the published data from ChemSpider (Royal Society of Chemistry, 2015).

$$n = \frac{N}{1 + N(e)^2} \tag{6.1}$$

6.4 Results and Discussion

6.4.1 Catalyst Characterization

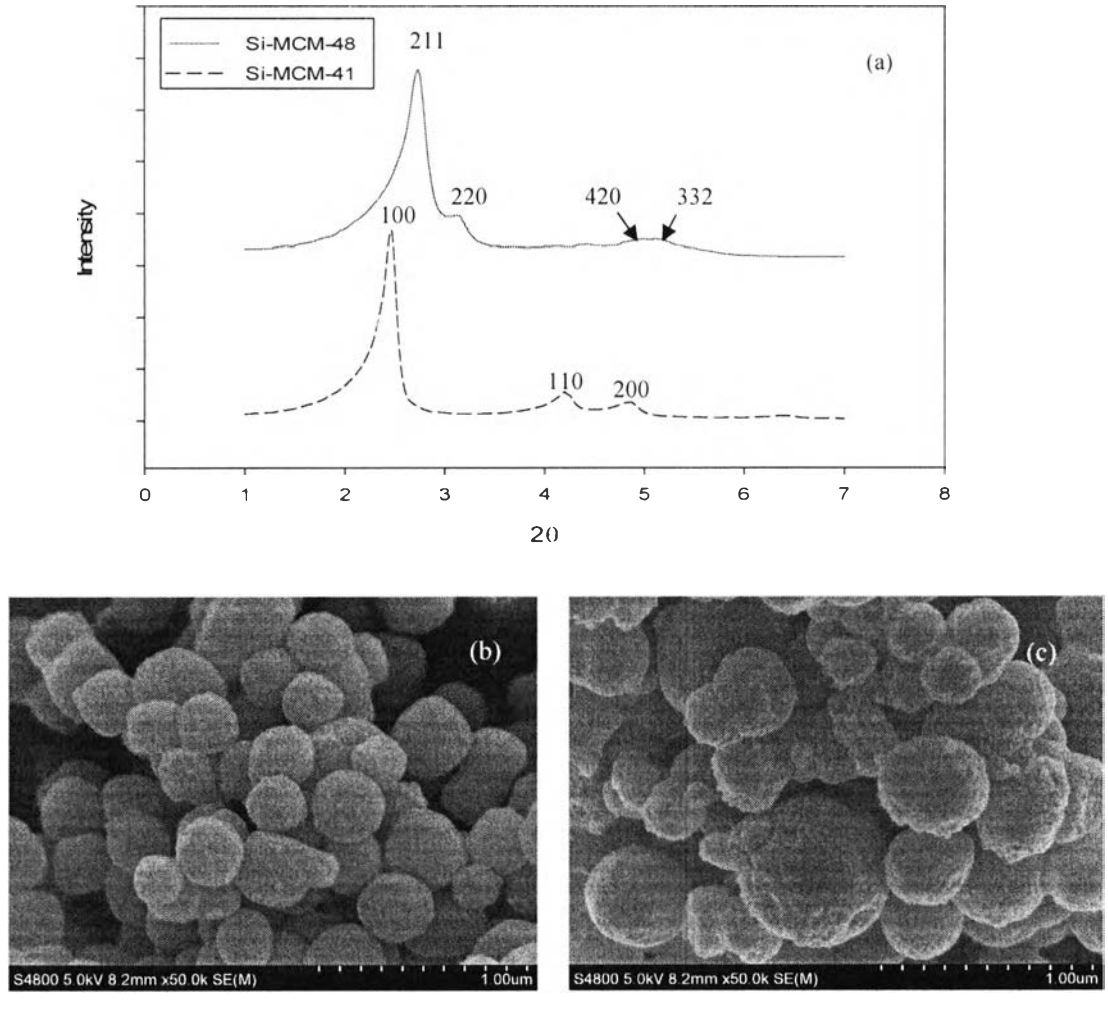

Figure 6.1 (a) SAXS patterns, and FE-SEM images of synthetic (b) Si-MCM-41 and (c) Si-MCM-48.

The SAXS patterns of synthetic Si-MCM-41 and Si-MCM-48 in Figure 6.1a show a good uniform structure. The SAXS pattern of Si-MCM-41 presents three major diffraction peaks, corresponding to the planes (100), (110), and (200) that can be indexed to *P6mm* hexagonal structure (Mele´ndez-Ortiz *et al.*, 2012) whereas the pattern of Si-MCM-48 presents four characteristic diffraction

peaks, corresponding to the planes (211), (220), (420), and (332) that can be indexed to I*a3d* cubic structure (Meléndez-Ortiz *et al.,* 2014). Figures 6.1b-6.1c show FE-SEM micrographs of Si-MCM-41 and Si-MCM-48, exhibiting that the molecular sieves have the similar morphology. However, Si-MCM-48 has larger cluster sizes than Si-MCM-41.

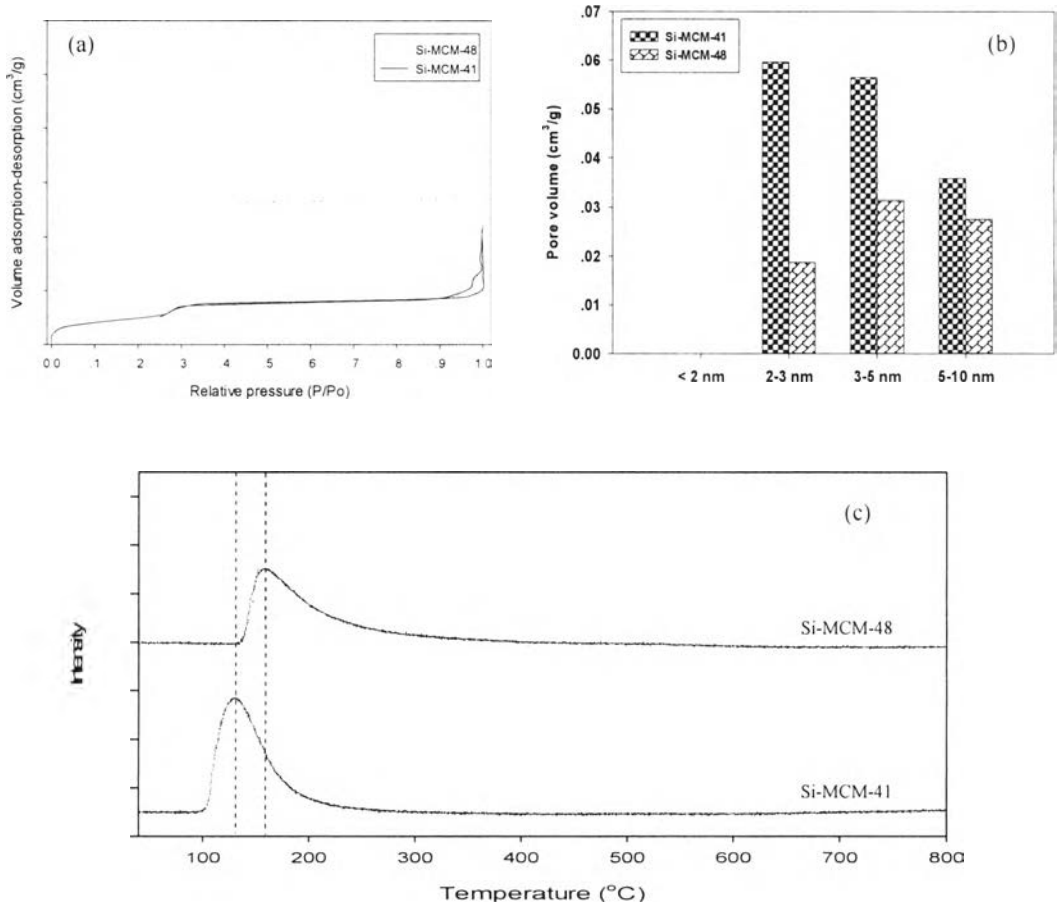

Figure 6.2 (a) Isotherms, (b) pore size distributions, and (c) TPD-NH_3 profiles of synthetic Si-MCM-41 and Si-MCM-48.

Figure 6.2a displays the nitrogen sorption isotherm and pore size distribution of synthetic Si-MCM-41 and Si-MCM-48. The typical type IV sorption isotherms of Si-MCM-41 and Si-MCM-48 are observed, according to IUPAC classification, indicating typical H1 hysteresis loop for mesoporous materials. The pore diameters are mostly distributed in the range of 2-10 nm as seen in Figure 6.2b.

The TPD-NH_3 profiles are illustrated in Figure 6.2c. The profiles of Si-MCM-41 and Si-MCM-48 show a small unique peak with the maximum at 133 °C and 152 °C, respectively, exhibiting that both Si-MCM-41 and Si-MCM-48 have a low amount of total acid site. Si-MCM-41 and Si-MCM-48 structures are constructed from association of pure silica, which is dominated by the presence of hydroxide groups referred as silanol groups (Simpson, 2015); thus, the acidity must be contributed from the silanol groups as seen in Figure 6.3. Therefore, the NH_3-desorption peak of Si-MCM-41 at 133 °C, which is lower than that of Si-MCM-48 (152 °C), indicates that the silanol groups on Si-MCM-41 have weaker acid strength.

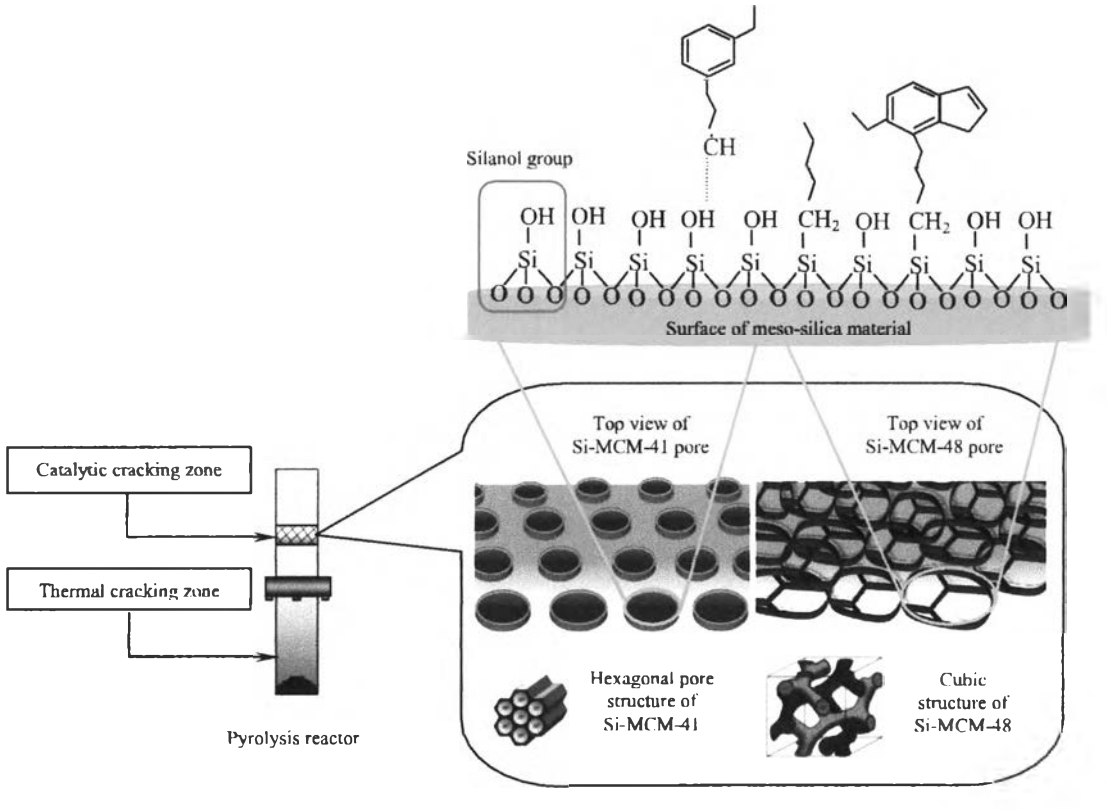

Figure 6.3 Silanol groups on the surfaces of mesoporous Si-MCM-41 and Si-MCM-48.

The porous properties of catalysts deduced from the nitrogen sorption isotherm are summarized in Table 6.1. The unit cell of hexagonal structure for Si-MCM-41 can be calculated from $a_0 = 2d_{100}/\sqrt{3}$ whereas the cubic structure for Si-MCM-48 can be calculated from $a_0 = d_{211} (h^2 + k^2 + l^2)^{1/2}$, where the d spacing of Si-MCM-41 and MCM-48 appears at plane (100) and (211), respectively (Meléndez-Ortiz *et al.*, 2014; Kibombo *et al.*, 2014). Since d-spacing can roughly indicate the pore size of molecular sieves, Si-MCM-41 and Si-MCM-48 pores are thus reported in the similar size (Lin *et al.*, 2014). Next, the synthetic molecular sieve Si-MCM-41 (hexagonal structure) and Si-MCM-48 (cubic structure), which have the similar pore size, were tested for their activity in pyrolysis of waste tire in order to investigate the effect of pore structure.

Table 6.1 Porous properties of synthesized Si-MCM-41 and Si-MCM-48

Mesoporous Materials	d[a] (nm)	a_0[b] (nm)	BJH Pore Diameter (nm)	Specific Pore Volume (cm^2/g)	S_{BET} (m^2/g)
Si-MCM-41	3.59	4.15	2.70	0.70	1,015
Si-MCM-48	3.32	8.13	2.78	0.70	940

[a] d_{100} for Si-MCM-41 and d_{211} for Si-MCM-48.
[b] $a_0 = 2d_{100}/\sqrt{3}$ for Si-MCM-41 and $a_0 = d_{211} (h^2 + k^2 + l^2)^{1/2}$ for Si-MCM-48

6.4.2 Effect of Pore Structure on Waste Tire Pyrolysis Products

Pyrolysis products can be divided into three types based on their phase; that are, gas, liquid, and solid or pyrolytic char as seen in Figure 6.4a. It shows that both Si-MCM-41and Si-MCM-48 suppress the gas yield. However, the coke formation on Si-MCM-48 is higher than that on Si-MCM-41, indicating that activity on the surface of Si-MCM-48 catalyst is higher than on Si-MCM-41. For gas composition as seen in Figure 6.4b, both Si-MCM-41 and Si-MCM-48 significantly increase methane, ethane, and propane, whereas mixed-C4 and mixed-C5 are significantly reduced.

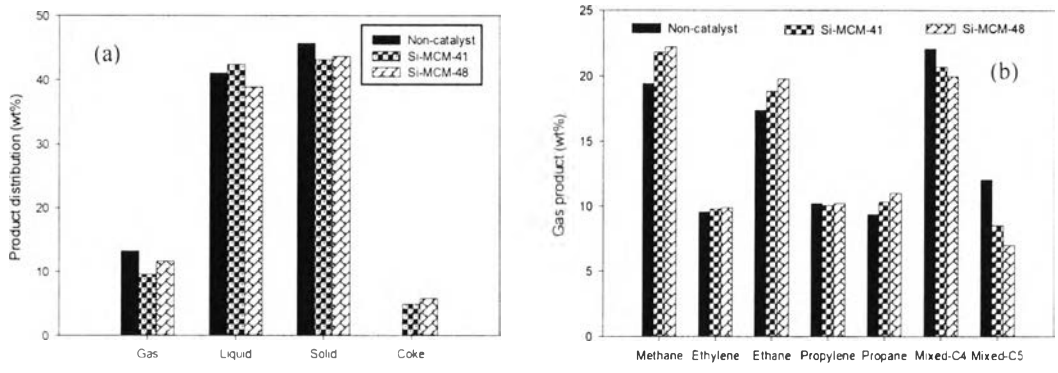

Figure 6.4 (a) Product distribution, and (b) gas compositions from using synthesized Si-MCM-41 and Si-MCM-48.

Asphaltene were separated from the liquid products prior to analysis with SIMDIST GC and GCxGC/TOF-MS in order to solve the interference of the overlap peak of complex hydrocarbons (Dijkmans *et al.*, 2015). The liquid products of all cases contain approximately 0.1-0.2 wt% of asphaltene. The petroleum fractions obtained from Si-MCM-41 and Si-MCM-48 are displayed in Figure 6.5. It can be observed that both Si-MCM-41 and Si-MCM-48 dramatically decrease heavy fractions (LVGO, and HVGO) in oil by 63.6 % and 79.8 %, respectively. Also, gas oil is reduced using both molecular sieves by 24.5 % and 36.0 %, respectively, which therefore drastically enhances the gasoline content by approximately three times for Si-MCM-41 case and four times for Si-MCM-48 case, and increases the kerosene content by 38.8 % of Si-MCM-41 case and 44.9 % for Si-MCM-48 case.

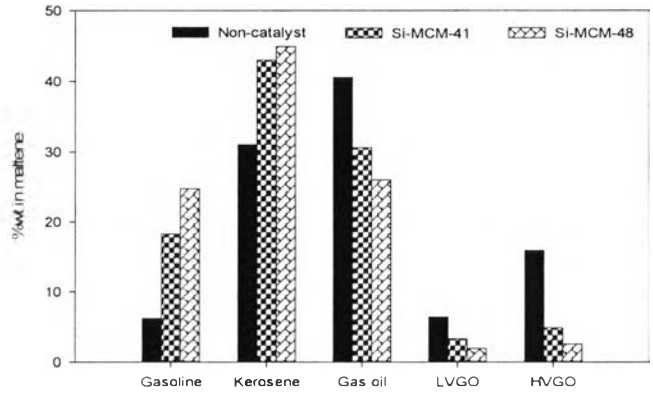

Figure 6.5 Petroleum fraction from using synthesized Si-MCM-41 and Si-MCM-48.

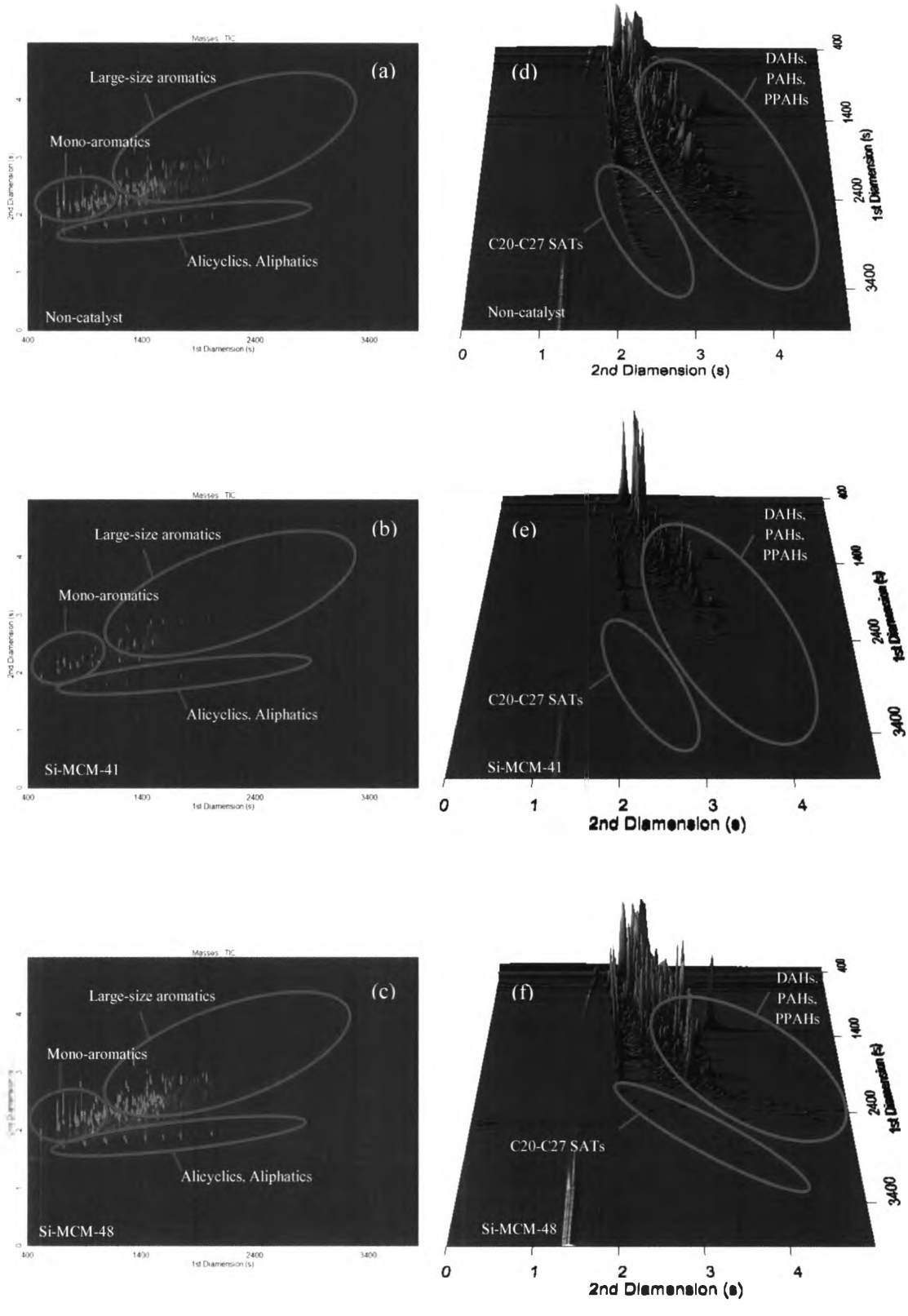

Figure 6.6 Total Ion Chromatograms of maltenes: contour plots (2D) in cases of (a) non-catalyst, (b) Si-MCM-41, and (c) Si-MCM-48, and surface plots (3D) in cases of (d) non-catalyst, (e) Si-MCM-41, and (f) Si-MCM-48.

Figures 6.6a-6.6b displays the contour plots of TICs of maltenes, which depict the distribution of hydrocarbon species that can be classified based on their structure into three mains categories; that are, aliphatics, alicyclics, and aromatics. After using Si-MCM-41 and Si-MCM-48 catalysts, the intensities of large-size aromatics (DAHs, PAHs, and PPAHs) in surface plots (Figures 6.6e-6.6f) is dropped as compared to those of non-catalyst case. It means that the concentration of these compounds is decreased by using mesoporous Si-MCM-41 and Si-MCM-48. The results can be confirmed by the distribution of molecular compositions as seen in Figure 6.7. It is found that Si-MCM-41 and Si-MCM-48 drastically decrease multi-ring aromatics (DAHs, PAHs, and PPAHs), and increase MAHs, TERs, NAPs, and OLEs, except SATs, especially C20-C27.

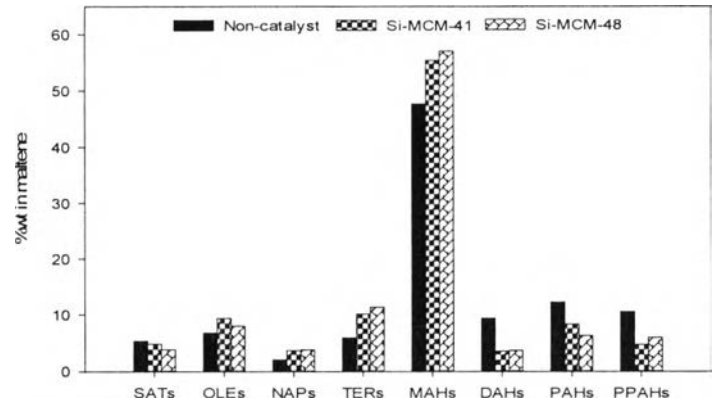

Figure 6.7 Molecular compositions of maltenes from using synthesized Si-MCM-41 and Si-MCM-48.

Next, the molecular composition in each petroleum cut was determined so that the quality of each cut can be predicted. The number of representatives of each molecular group needed for the calculation was first determined from Yamane method (Israel, 2013) as shown in Table 6.2. Out of more than 800 species that are normally detected in TDOs, the number of sampling size is in the range of 365-398 species, accounting for 86.8-89.0 % of total sampling area. Moreover, the area percentage of samples in each group shows that the sampling was well handled. Then, the molecular compositions in each petroleum cut were calculated as reported in Table 6.3.

Table 6.2 Sampling size and representatives from each molecular group of compounds

Molecular Group	Number of Detected Compounds			Number of Sampling Size[a]			%Area of Detected Compounds			%Area of Sampling		
	1	2	3	1	2	3	1	2	3	1	2	3
SATs	42	63	66	30	39	40	5.3	4.9	3.9	5.2	4.7	3.8
OLEs	110	128	129	52	56	56	7.4	9.1	8.1	6.2	8.0	7.1
NAPs	42	80	86	30	44	46	2.0	3.4	3.8	1.9	3.0	3.5
TERs	100	146	151	50	59	60	6.7	10.5	11.4	5.8	9.1	10.1
MAHs	231	248	213	70	71	68	46.9	55.3	56.7	40.6	45.9	49.1
DAHs	27	25	25	21	20	20	9.2	3.6	3.7	9.2	3.6	3.7
PAHs	96	104	95	49	51	49	12.1	8.5	6..3	11.2	7.9	6.1
PPAHs	174	115	140	64	53	58	10.4	4.8	6.0	9.0	4.5	5.8
Total	822	909	905	365	394	398	100	100	100	89.0	86.8	89.0

[a]Yamane (Israel, 2013), 1 = Non-catalyst, 2 = Si-MCM-41, 3 = Si-MCM-48

Table 6.3 shows the relationship between petroleum fractions and molecular components in each petroleum cut. Molecular components were arranged based on their boiling points (Royal society of chemistry, 2015) into each petroleum fraction. It is clearly seen that gas oil and vacuum gas oil (LVGO and HVGO) fractions from thermal decomposition are mainly composed of 58.1 % multi-ring aromatics (DAHs, PAHs, and PPAHs), followed by 23.9 % mono-aromatics (MAHs), 14.4 % aliphatics (SATs and OLEs), and 3.6 % alicyclics (NAPs and TERs). Both Si-MCM-41 and Si-MCM-48 can decrease 41.2-48.9 % multi-ring aromatics in gas oil and vacuum gas oil, and increase 77.2-61.5 % of alicyclics, 30.6-32.7 % of mono-aromatics, and 15.7-35.8 % of aliphatics in gasoline and kerosene fractions. It indicates that the reduction of multi-ring aromatics in gas oil and vacuum gas oil leads to the enhancement of gasoline and kerosene qualities.

3 Molecular composition of each petroleum cuts (wt%) in maltenes from Si-MCM-41 and Si-MCM-48 cases (1 = Non-
2 = Si-MCM-41, and 3 = Si-MCM-48)

arbon group	Gasoline			Kerosene			Gas oil			LVGO			HVGO		
	1	2	3	1	2	3	1	2	3	1	2	3	1	2	3
	0.14	0.16	0.08	1.82	2.31	1.90	2.21	2.67	1.51	1.09	-	0.76	0.52	0.30	0.01
	1.34	1.00	1.66	3.12	5.26	3.79	2.51	2.86	1.75	-	0.14	0.77	-	-	-
	0.15	0.24	0.59	1.80	2.58	2.93	0.20	0.69	0.39	-	-	-	-	-	-
	0.64	0.41	1.29	4.47	8.19	7.71	1.35	1.85	2.32	0.05	-	-	-	-	-
	2.43	7.45	5.84	32.68	38.38	40.74	10.51	7.17	8.56	-	-	-	-	-	-
	-	-	-	1.92	-	0.01	8.32	4.09	4.10	-	0.01	0.02	-	0.02	-
	-	-	-	-	-	-	10.36	7.70	6.10	1.29	0.88	0.45	0.92	0.51	0.29
	0.17	0.12	0.27	5.27	3.20	4.02	3.59	1.59	1.68	0.73	0.13	0.21	0.38	0.10	0.24
	4.8"	**9.3"**	**9."4**	**51.08**	**59.92**	**61.10**	**39.0"**	**28.62**	**26.42**	**3.1"**	**1.16**	**2.21**	**1.82**	**0.93**	**0.54**

Table 6.4 Ultimate analysis (wt%) of oil products

Ultimate Analysis[a] (wt%)	C	H	C/H Ratio
Non-catalyst	69.10±0.42	9.62±0.15	7.19
Si-MCM-41	64.75±1.20	9.84±0.04	6.58
Si-MCM-48	61.80±0.28	9.83±0.24	6.29

Alicyclic hydrocarbons in gasoline and kerosene are greatly increased, indicated also from the decrement of C/H ratio as reported in Table 6.4, meaning that Si-MCM-41 and Si-MCM-48 can be used to enhance the hydrogenation of aromatic compounds. Since the bonding energy of C-H bond is very low (88.5 kcal/mol); thus, hydrogen from thermal cracking reaction can be easily produced (Malvin and Poutsma, 2000; Shi and Que, 2003). However, the main reaction in pyrolysis of waste tire for both thermal and catalyst decompositions is cracking, favored at β-scission (Choi *et al.*, 2000; Chen *et al.*, 2002). Moreover, the C-C bond breaking of aromatic rings via ring-opening reaction can be enhanced by functions of metals such as Pt (Dũng *et al.*, 2009a), Ru (Dũng *et al.*, 2009b), and Cu (Yuwapornpanit and Jitkarnka, 2015), implying that it may not be easy for using only mesoporous materials to directly break C-C bond of aromatic hydrocarbons even though mesoporous materials can provide a high mass diffusion into their pores. Therefore, the decrement of DAHs, PAHs and PPAHs by using mesoporous Si-MCM-41 and Si-MCM-48 may be resulted from the cracking via silanol groups in their pores, as seen in Figure 6.3. Seddegi *et al.* (2002) proposed that the silanol groups in the channels of these materials can provide ions to molecules; causing the increment of molecular adsorption on surface, and then the molecules were stabilized in carbenium ions form that subsequently undergo further reaction.

6.4.3 Proposed Schemes of Mono-aromatic Formation

In addition, a strong increase in mono-aromatics in gasoline and kerosene using Si-MCM-41 and Si-MCM-48 may be resulted from hydrogenation of multi-ring aromatic hydrocarbons prior to ring opening. The dominant aromatic hydrocarbons, which are significantly found influenced by the silanol groups in the pore of Si-MCM-41 and Si-MCM-48, are shown in Table 6.5. Three possible

schemes for conversion of di-, poly-, and polar-aromatics into mono-aromatics and some petrochemicals using mesoporous Si-MCM-41 and Si-MCM-48 are hereby proposed as shown in Figure 6.8.

Table 6.5 Dominant aromatic compounds found in TDOs from using synthesized Si-MCM-41 and Si-MCM-48

Chemical Name	Exact mass (m/z)	% Area		
		Non-cat.	Si-MCM-41	Si-MCM-48
Mono-aromatics (MAHs)				
Benzene	78.0469	-	-	0.57
Toluene	92.0626	-	1.73	1.39
Ethylbenzene	106.0782	1.50	4.49	1.55
Mixed-xylenes	106.0782	0.19	1.34	1.55
Styrene	104.0626	0.52	0.07	3.96
Cumene	120.0939	0.18	3.20	3.12
2-ethyltoluene	120.0939	0.06	1.43	1.00
Methylstyrene	118.0782	0.71	1.62	2.05
Propylbenzene	120.0939	-	1.56	1.20
1,2,3,4-tetrahydro-5-methyl-		-	0.05	0.06
Naphthalene	146.1095			
Di-aromatics (DAHs)				
1-methyl-naphthalene	142.0782	3.14	1.22	1.29
Poly-aromatics (PAHs)				
4-methyl-1,1'-biphenyl	168.0939	1.73	0.72	1.00
Biphenyl	154.0782	1.60	0.83	0.64
1,1'-(1,3-propanediyl)bis-benzene	196.1252	1.32	0.88	0.90
4-(1-methylethyl)- 1,1'-biphenyl	196.1252	0.37	0.19	0.19
Polar-aromatics (PPAHs)				
Benzothiazole	135.0142	2.44	1.08	1.41
Isothiocyanato-benzene	135.0142	-	0.60	0.53

Scheme 1: Di-aromatics to mono-aromatics

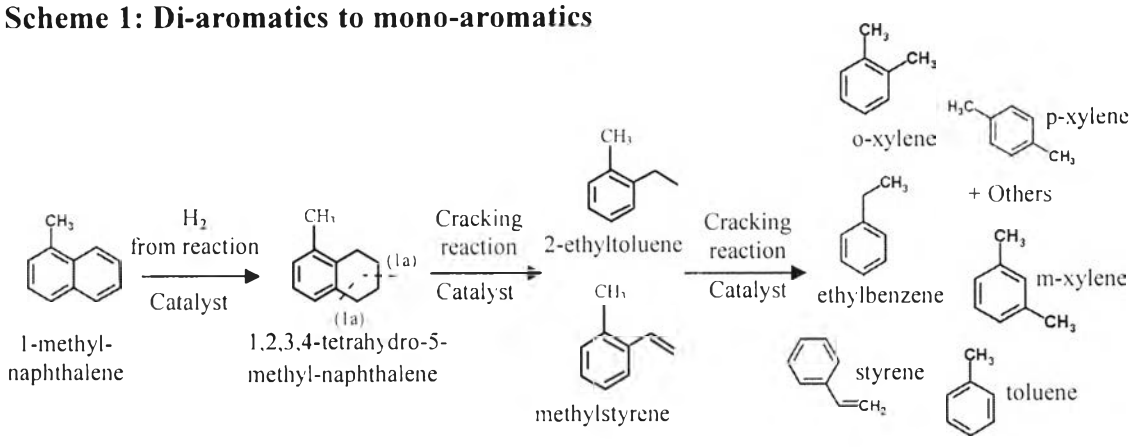

Scheme 2: Poly-aromatics to mono-aromatics

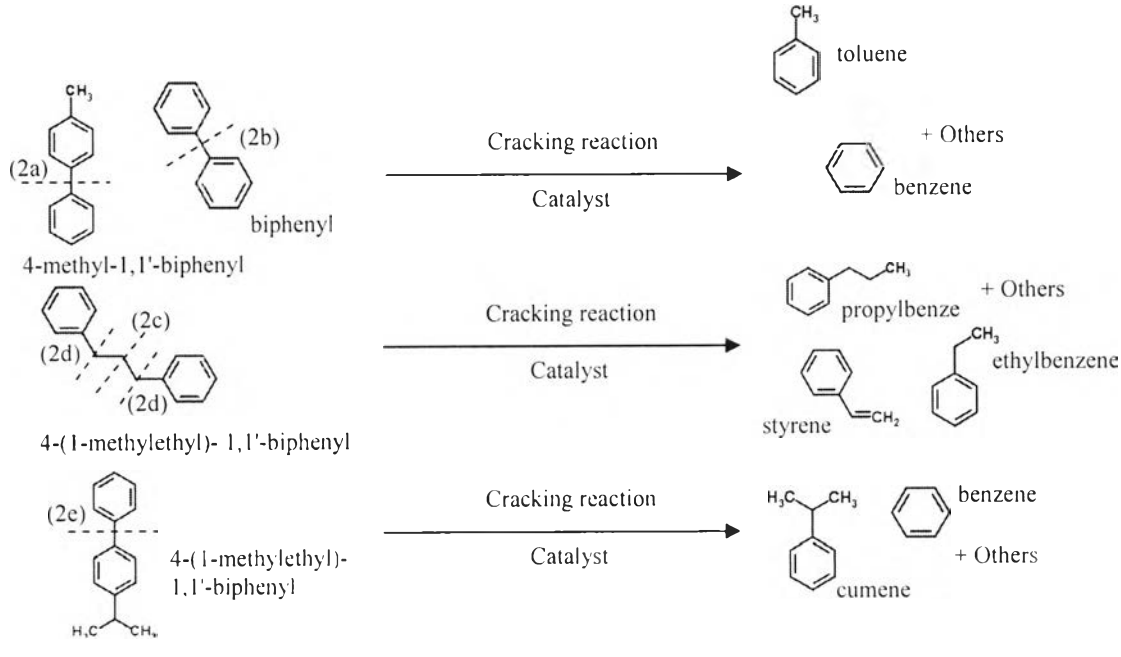

Scheme 3: Polar-aromatics to mono-aromatics

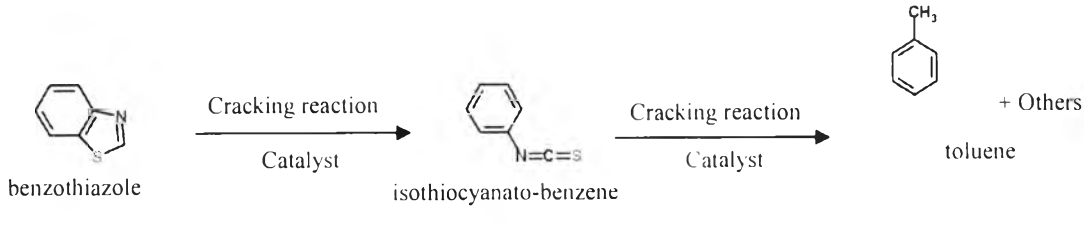

Figure 6.8 Proposed reaction schemes for conversion of di-, poly-, and polar-aromatics into mono-aromatics using synthesized mesoporous Si-MCM-41 and Si-MCM-48.

Scheme 1 displays the transformation of dominant di-aromatic species to mono-aromatic compounds. 1-methyl-naphthalene, found decreased using both mesoporous catalysts, may be first hydrogenated in the pore of both mesoporous catalysts. If the C-C scission takes place at the position **1a**, 2-ethyltoluene and methylstyrene are then the possible dominant mono-aromatic products. Subsequently, ethylbenzene, styrene, mixed-xylenes, toluene, and non-aromatics can be formed by cracking of 2-ethyltoluene and methylstyrene. Si-MCM-41 favors to produce 2-ethyltoluene and ethylbenzene whereas Si-MCM-48 more selectively produces methylstyrene and styrene. Furthermore, m-xylene and p-xylene can be formed by the isomerization of o-xylene.

Scheme 2 presents the transformation of some dominant poly-aromatic species to mono-aromatic compounds. For examples, 4-methyl-1,1'-biphenyl and biphenyl can be cracked, forming benzene, toluene, and non-aromatics. However, the concentration of benzene is dramatically reduced, indicating that benzene radical might react with other hydrocarbon radicals to form toluene or other compounds. Furthermore, ethylbenzene and propylbenzene can be formed by cracking of 4-(1-methylethyl)-1,1'-biphenyl at the positions **2c** and **2d**, respectively. However, ethylbenzene is more selectively produced because of a high increase in its concentration in the Si-MCM-41 case. For the Si-MCM-48 case, ethylbenzene can be converted to styrene via dehydrogenation, causing an extremely low ethylbenzene concentration and a great increase in styrene concentration in the maltene solution. Moreover, 4-(1-methylethyl)-1,1'-biphenyl can be cracked at the position **2c** to form cumene, benzene, and non-aromatics.

Scheme 3 exhibits the transformation of dominant polar-aromatic species to mono-aromatic compounds. Interestingly, the synthesized mesoporous Si-MCM-41 and Si-MCM-48 can directly open the ring of polar-aromatics (PPAHs) at the carbon-heteroatom position, resulting in an extreme decrease in benzothiazole and an increase in isothiocyanato-benzene. This may be possibly caused by a weak bonding energy between a carbon and a heteroatom (C-S; 65 kcal/mol, and C-N; 73 kcal/mol); thus, the C-heteroatom bonds can be more easily broken than C-C bond (102 kcal/mol) (Malvin and Poutsma, 2000) in a ring of polar-aromatics. Therefore, toluene can be formed by cracking of benzothiazoles.

6.4.4 Petrochemical Productivity

To gain insight into the detail of mono-aromatic formation, the percentage of petrochemicals in mono-aromatics is shown in Figure 6.9. It can be observed that Si-MCM-41 enhances the concentration of petrochemicals in mono-aromatics from 5.0 % to 10.5 % whereas the use of Si-MCM-48 results in 11.7 % petrochemicals in mono-aromatics. Both mesoporous catalysts do not give significantly different petrochemical contents in mono-aromatics. In details, the results show that Si-MCM-41 produces toluene and ethylbenzene with the highest amount whereas Si-MCM-48 produces benzene and styrene with the highest amount. The other compounds are produced with a similar concentration with using Si-MCM-41 and Si-MCM-48. The difference in petrochemical products produced by Si-MCM-41 (hexagonal) and Si-MCM-48 (cubic) might be caused by the difference of pore structure that influences reaction time and steric hindrance of reacting molecules inside the pores. However, Si-MCM-48 can enhance petrochemical production more slightly than Si-MCM-41 as reported in Table 6.6 although the productivity of both mesoporous catalysts is not significantly different. One possible explanation is that the acid strength of silanol groups on Si-MCM-48 is slightly stronger than those on Si-MCM-41 as observed in Figure 6.2c in association with its more complex cubic structure.

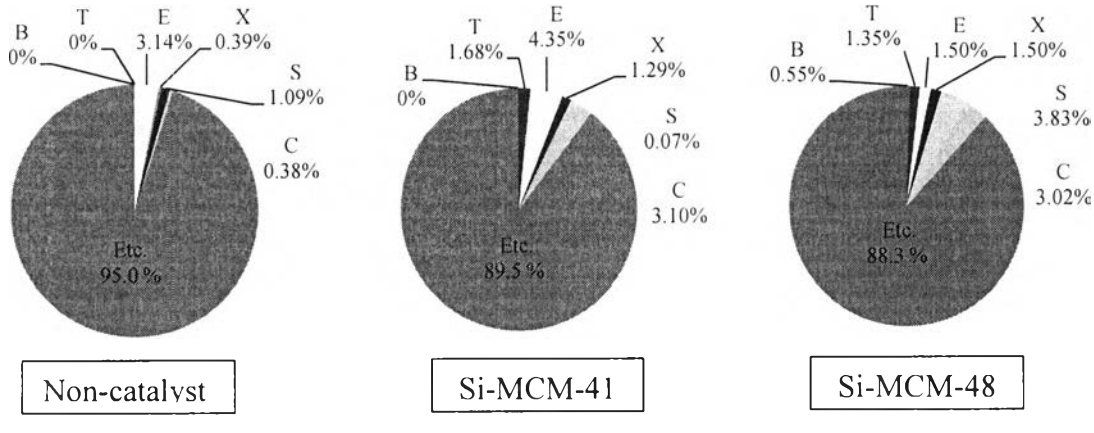

Figure 6.9 Percentage of petrochemicals in mono-aromatic fraction (B = Benzene, T = Toluene, E = Ethylbenzene, X = Mixed-xylenes, S = Styrene, and C = Cumene).

Table 6.6 Petrochemical productivity from waste tire pyrolysis

Catalyst	Petrochemical Productivity (kg/ton of tire)
Non-catalyst	9.8
Si-MCM-41	24.6
Si-MCM-48	26.1

According to the results, it can be summaried that the molecule of tire is decomposed into smaller compounds at the thermal cracking zone. The obtained product has high contents of aromatics (MAHs, DAHs, PAHs, and PPAHs), followed by aliphatic (SATs and OLEs) and alicyclic (NAPs and TERs) compounds. Then, all of components are transferred to the catalytic zone (the upper zone of reactor) as seen in Figure 6.3, where the molecules are reformed. Moreover, the high porosity of Si-MCM-41 and Si-MCM-48 can contribute to the high diffusion of large-size aromatics with high boiling points to the pore. Subsequently, the molecules from thermal cracking at the pyrolytic zone are protonated by the silanol groups on Si-MCM-41 and Si-MCM-48 structures, forming carbenium ions that subsequently undergo further cracking reactions. Therefore, the products are lighter than the non-catalyst case. However, the Si-MCM-48 is likely to have better catalytic cracking performance than the Si-MCM-41 since it more greatly converts gas oil, HVGO, and LVGO, leading to the lighter liquid product. In addition, Si-MCM-41 and Si-MCM-48 can greatly reduce sulfur content in TDOs. However, Si-MCM-48 shows a higher decrease in both sulfur and nitrogen than Si-MCM-41 as seen in Table 6.7. It indicates that the Si-MCM-48 catalyst can convert sulfur and nitrogen compounds in TDO to other products via cracking reaction and hydrogenation better than the Si-MCM-41 catalysts. The results indicate that the cubic pore structure of Si-MCM-48 allows molecules to stay inside the meso-pore channel with a longer residence time, and then heavy fractions can be cracked into lighter fractions more effectively than in the hexagonal structure of Si-MCM-41.

Table 6.7 Ultimate analysis of hetero-atom (S,N) contents in tire-derived oils

Ultimate Analysis (wt%)	S	N
Non-catalyst	1.27±0.00	0.40±0.04
Si-MCM-41	0.88±0.03	0.40±0.02
Si-MCM-48	0.84±0.01	0.34±0.01

6.5 Conclusions

In this research work, mesoporous Si-MCM-41 and Si-MCM-48 were synthesized, and then used in waste tire pyrolysis. The synthesis at room temperature can yield the good uniform hexagonal and cubic structures of Si-MCM-41 and Si-MCM-48, respectively. For catalytic reaction, both catalysts can highly decrease gas oil and vacuum gas oil fractions, leading to a substantial enhancement of gasoline and kerosene. Interestingly, both Si-MCM-41 and Si-MCM-48 with low acidity can open rings of aromatics because the large porosity of Si-MCM-41 and Si-MCM-48 can contribute the diffusion of large-size aromatics, especially di-, poly-, and polar-aromatics with high boiling points to the pore. Consequently, the silanol groups in the pore of Si-MCM-41 and Si-MCM-48 can protonate the molecules in tire-derived oil, forming carbenium ions. However, the cubic structure gave higher removal of heavy compounds because its three-dimensional interconnected cubic pore structure created slightly-stronger silanol groups, and consequently performed reaction with a higher retention time inside the pore. Nevertheless, both mesoporous catalysts did not give significantly different production of petrochemicals even though the compositions of petrochemicals components were somewhat different. Finally, three schemes were proposed to explain the formation of mono-aromatics of petrochemicals, based on the GCxGC/TOF-MS results observed from using both mesoporous catalysts. Interestingly, these two materials can drastically reduce sulfur content in oil. However, Si-MCM-48 not only more greatly removes sulfur but also nitrogen in oil than Si-MCM-41.

6.6 Acknowledgements

The authors would like to thank The Petroleum and Petrochemical College, Chulalongkorn University, Thailand, Center of Excellence on Petrochemical and Materials Technology, and Thailand Research Fund (TRF: RSA5680021) for all supports.

6.7 References

Chen, F. and Qian, J. (2002) Studies on the thermal degradation of cis-1,4-polyisoprene. Fuel, 81, 2071–2077.

Choi, S.S. (2000) Characterization of bound rubber of filled styrene–butadiene rubber compounds using pyrolysis-gas chromatography. Journal of Analytical and Applied Pyrolysis, 55, 161–170.

Dijkmans, T., Djokic, M.R., Geem, K.M.V., and Marin, G.B. (2015) Comprehensive compositional analysis of sulfur and nitrogen containing compounds in shale oil using GCxGC-FID/SCD/NCD/TOF-MS. Fuel, 140, 398-406.

Dũng, N.A., Wongkasemjit, S., and Jitkarnka, S. (2009a) Effects of pyrolysis temperature and Pt-loaded catalysts on polar-aromatic content in tire-derived oil. Applied Catalysis B: Environmental, 91, 300-307.

Dũng, N.A., Klaewkla, R., Wongkasemjit, S., and Jitkarnka, S. (2009b) Light olefins and light oil production from catalytic pyrolysis of waste tire. Journal of Analytical and Applied Pyrolysis, 86, 281–286.

Israel, G.D. (2013) Determining Sample Size. Florida: University of Florida.

Jin, S., Cui, K., Guan, H., Yang, M., Liu, L., and Lan, C. (2012) Preparation of mesoporous MCM-41 from natural sepiolite and its catalytic activity of cracking waste polystyrene plastics. Applied Clay Science, 56, 1–6.

Kibombo, H.S., Balasanthiran, V., Wu, C.M., Peng, R., and Koodali, R.T. (2014) Exploration of room temperature synthesis of palladium containing cubic MCM-48 mesoporous materials. Microporous and Mesoporous Materials, 198, 1-8.

Lin, J., Zhao, B., Cao, Y., Xu, H., Ma, S., Guo, M., Qiao, D., and Cao, Y. (2014) Rationally designed Fe-MCM-41 by protein size to enhance lipase immobilization, catalytic efficiency and performance. Applied Catalysis A: General, 478, 175–185.

Marvin, L. and Poutama. (2000) Fundamental reactions of free radicals relevant. Journal of Analytical and Applied Pyrolysis, 54, 5-35.

Meléndez-Ortiz, H.I., Perera-Mercado, Y., Mercado-Silva, J.A., Olevares-Maldonado, Y., Castruita, G., and García-Cerda, L.A. (2014) Functionalization with amine-containing organosilane of mesoporous silica MCM-41 and MCM-48 obtained at room temperature. Ceramics International, 40, 9701-9707.

Pithakratanayothin, S. and Jitkarnka, S. (2014) Comparison of Components in Oil Derived from Tyre Pyrolysis with and without KL Catalyst Using GC×GC/TOF-MS. Chemical Engineering Transaction, 39, 1261-126.

Royal Society of Chemistry. "ChemSpider." 2015. 20 October 2014 <www.ChemSpider.com>

Seddegi, S.Z., Budrthumal, U., Al-Arfaj, A.A., Al-Amer, A.M., and Barri, S.A. (2002) Catalytic cracking of polyethylene over all-silica MCM-41 molecular sieve. Applied Catalysis A: General, 225, 167–176.

Seng-eiad, S. and Jitkarnka, S. (2015) Estimation of average kinetic and maximum diameters of hydrocarbon groups in tyre-derived oil for catalyst design purpose. Chemical Engineering Transaction. (in press)

Shi, B. and Que, G. (2003) Cracking and cracking selectivity of alkane and alkyl aromatics: effects of dispersed catalysis and hydrogen donors. American Chemical Society, 48(2), 631-633.

Simpson, N.J.K. "Solid Phase Extraction." 2015. 20 March 2015 <http://www.slideshare.net/RonaldTalvat/solid-phase-extraction-principles-techniques-and-application>

Witpathomwong, C., Longloilert, R., Wongkasemjit, S., and Jitkarnka, S. (2011) Improving light olefins and light oil production using Ru/MCM-48 in catalytic pyrolysis of waste tire. Energy Procedia, 9, 245 – 25.

Yuwapornpanit, R. and Jitkarnka, S. (2015) Cu-doped catalysts and their impacts on tire-derived oil and sulfur removal. Journal of Analytical and Applied Pyrolysis, 111, 200-208.